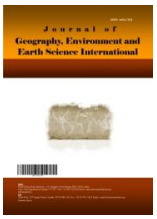

Journal of Geography, Environment and Earth Science International

24(5): 11-29, 2020; Article no.JGEESI.58030
ISSN: 2454-7352

Application of Aeromagnetic Data to Assess the Structures and Solid Mineral Potentials in Part of North Central Nigeria

M. D. Tawey[1*], D. U. Alhassan[2], A. A. Adetona[2], K. A. Salako[2], A. A. Rafiu[2] and E. E. Udensi[2]

[1]National Water Resources Institute, Mando Road Kaduna, Nigeria.
[2]Department of Geophysics, Federal University of Technology Minna, Nigeria.

Authors' contributions

This work was carried out in collaboration among all authors. Author MDT designed the study, performed the statistical analysis, wrote the protocol and wrote the first draft of the manuscript. Authors DUA, AAA and KAS managed the analyses of the study. Authors AAR and EEU managed the literature searches. All authors read and approved the final manuscript.

Article Information

DOI: 10.9734/JGEESI/2020/v24i530223
Editor(s):
(1) Dr. Pere Serra Ruiz, Universitat Autònoma de Barcelona, Spain.
Reviewers:
(1) Aymen Adil Lazim, Iraq.
(2) Mounir Amar, Morocco.
Complete Peer review History: http://www.sdiarticle4.com/review-history/58030

Original Research Article

Received 20 April 2020
Accepted 25 June 2020
Published 06 July 2020

ABSTRACT

Assessment of the structures and solid minerals was carryout to investigate subsurface structural characteristics and mineralization potential zones within part of north-central Nigeria. The residual magnetic intensity data of the area was reduced to magnetic pole after which several source edge detection/interpretation with depth determination techniques including, analytic signal; tilt derivative; first and second vertical derivatives and Euler deconvolution were applied to the aeromagnetic data. From the analytic signal map, three magnetic zones were delineated. These are: low to relatively low magnetic zone (LM) with amplitude range from 0.003 to 0.009, moderate magnetic zone (MM) with amplitude 0.009 to 0.106 and those with amplitudes above 0.106 were products of later magmatic intrusions into host with fractures, faults and joints. Tilt derivative helped in delineating location and extent of edges of causative sources while Euler deconvolution helps in determination of boundary, depth and geometry of the structures. From first vertical derivative map,

**Corresponding author: E-mail: taweymam@gmail.com;*

structures were found to have high lineament density around the central portion of the area and span toward the western end of the map were delineated. The lineaments mapped trending in the ENE-WSW followed by WNW-ESE with some NE-SW, NNE-SSW and NNW-SSE trends. The second vertical derivative (SVD) map also helped in delineating structures and possible mineralization zones that are pronounced within the study area, around high analytic signal zones. Delineated possible and favorable mineralization zones from second vertical derivative map correlate with portion of the study area with rocks showing high analytic signal amplitude suggesting the rocks to be of later magmatic intrusions where mineralization fluids solidify within the host rocks.

Keywords: Mineralization; vertical derivative; source edge detection; structures.

1. INTRODUCTION

Broad aeromagnetic surveys have been used to locate faults, shear zones and fractures. Such zones may serve as potential hosts for a variety of minerals and may be used as guidance for the exploration of epigenetic, stress-related mineralization in the surrounding rocks [1]. According to [2], primary mineralization in Nigeria is largely lithological and structurally controlled. Solid mineral exploration requires interpretation of high-resolution airborne data, usually aimed at delineating possible rocks, zones and structures that may serve as hosts [3]. Several articles have been published on parts of central Nigerian Basement complex mineralogical and structural framework with depth to magnetic source based on interpretation of aeromagnetic data [4-7]. [7] carried out analysis of aeromagnetic data over Wamba and its adjoining areas in north-central Nigeria. The interpreted orientations or azimuth direction of the structural lineaments delineated on the maps depicted major trends being NE-SW, NW-SE and NNE-SSW (Pan-African trends) with minor NNW-SSE and E-W trends (pre-Pan-African trends). Depths to the magnetic source bodies were estimated using Peter's (half-slope) method, indicating two depth source models. The deeper sources ranged from 0.88 km to 3.15 km and had -32 nT to -225 nT magnetic intensity, whereas the shallower sources ranged from 0.23 km to 0.76 km and had -10nT to 20nT magnetic intensity. Also [5] carried out structural pattern deduction from aeromagnetic data over Parts of Nasarawa and Environs in North central Nigeria. The interpreted faults show criss-crossing pattern of fault zones, some of which appear to step over where they cross and show zones of west-northwest, north- and northwest-striking faults that cross west-northwest around Akiri warm spring. North easterly striking faults extend east from this juncture. They concluded that the associated aeromagnetic anomalies are likely caused by magnetic contrasts associated with rifting of crust beneath the Benue Trough. [6] carried out a reconnaissance study to delineate the potential mineral zones around the schist belt areas of Kano State north central Nigerian basement complex using airborne magnetic data. The short wavelength anomalies recorded in the study area, ranging from -99.182 to 88.338 nT which indicated that the area is characterized by crystalline basement complex rocks. The results of the vertical derivatives showed that lineaments (depicting faults, fractures and contacts) which represent veins of possible mineralization exist in the study area. The trend of these lineaments is in the NE-SW and E-W directions with the NE-SW trend dominating. According to [4], the mineralization zones located in the Shanono local government area of Kano state within north central Nigerian basement complex has its genesis controlled by shear zones. The research was aimed at delineating and characterizing subsurface geologic structures around the study area. Both qualitative and quantitative analysis of aeromagnetic data has provided defined distinct pattern of the magnetic signatures. Euler solution of the aeromagnetic data with structural index of one (SI=1), revealed the presence of the major tectonic trends of anomalies in the NE-SW and NW-SE directions. The trends of few of these structures are observed to be similar to fracture orientations in the Nigerian basement complex. These structures control the emplacement of the gold mineralization as these provides the pathways to flow of mineral rich fluid within the host rocks of the study area.

Nigeria is a country blessed with various mineral resources buried beneath the surface of the earth [8,9], but Nigeria depends solely on the crude oil. Solid minerals are not well harnessed to the country's economic advantage. The unstable price of crude oil has a great effect on the country's economy, and as the prolific Niger Delta's hydrocarbon potential is depleted or may be exhausted due to continuous exploitation in

the near future, attention needs to be shifted to other areas. Looking into our abundant, solid minerals is a good way to diversify the Nigeria's economy. In various parts of Nigeria there has been massive exploitation of minerals by local miners in an illegal and unprofessional manner. These mineral resources are supposed to benefit states and the country at large, but less has been done by the government to carry out the necessary geophysical study to review the quantity, types and depth of the mineral. This leaves the mining activities in the hands of illegal miners who have little or no knowledge about deposits beneath the earth. These local miners' activities have effects on the country's environment, health, safety and economy. Mineralisations presents a challenge for geophysical surveys this is because some of the mineralization itself does not provide a contrast with the host geology that is detectable by any of the geophysical parameters because of complex geology and structure [10]. Discovery of such deposits requires geophysical surveys that can detect subtle structures that control deposition and identify directly the weak anomalies created by processes of alteration and deposition.

This work used aeromagnetic data to interpret possible depth to geological structures (fractures, faults, folds and shear zones) and mapped potential mineralization zones associated with these structures within the research area.

The research area is located in the central part of Nigeria (Fig. 1) and bounded by latitude 8°30[1] N to latitude 10°30 [1] N with Longitude 7°E to Longitude 8°E.

The Nigerian basement complex is tectonically part of the Pan-African mobile belt and lies between the West African and Congo Cratons (Fig. 2) and south of the Tuareg Shield [11]. It has been intruded by the Mesozoic calc-alkaline ring complexes (Young Granites) of the Jos Plateau and is unconformably overlain by Cretaceous and younger sediments. The Nigerian basement (Fig. 3) was affected by the Pan-African orogeny of 600 Ma and occupies the reactivated region resulting from a plate collision between the passive continental margin of the West African craton and the active continental margin of Pharusian [12,13].

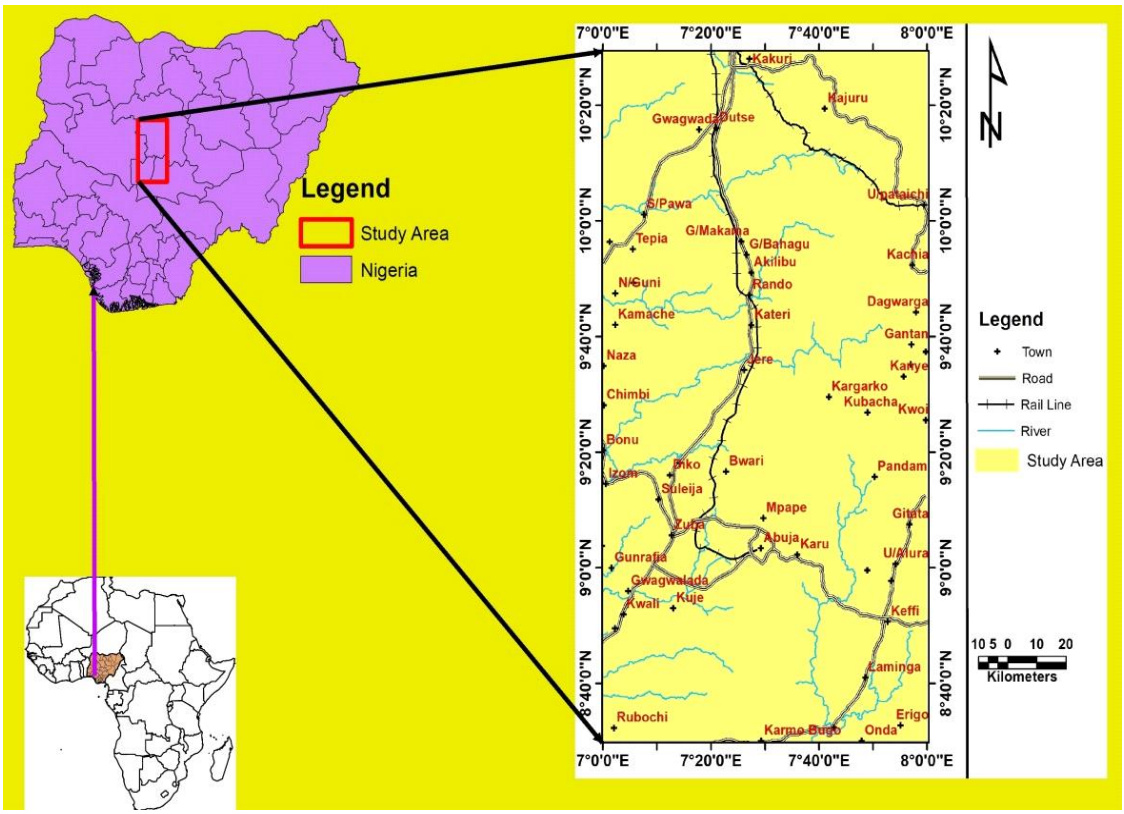

Fig. 1. Location map of the study area

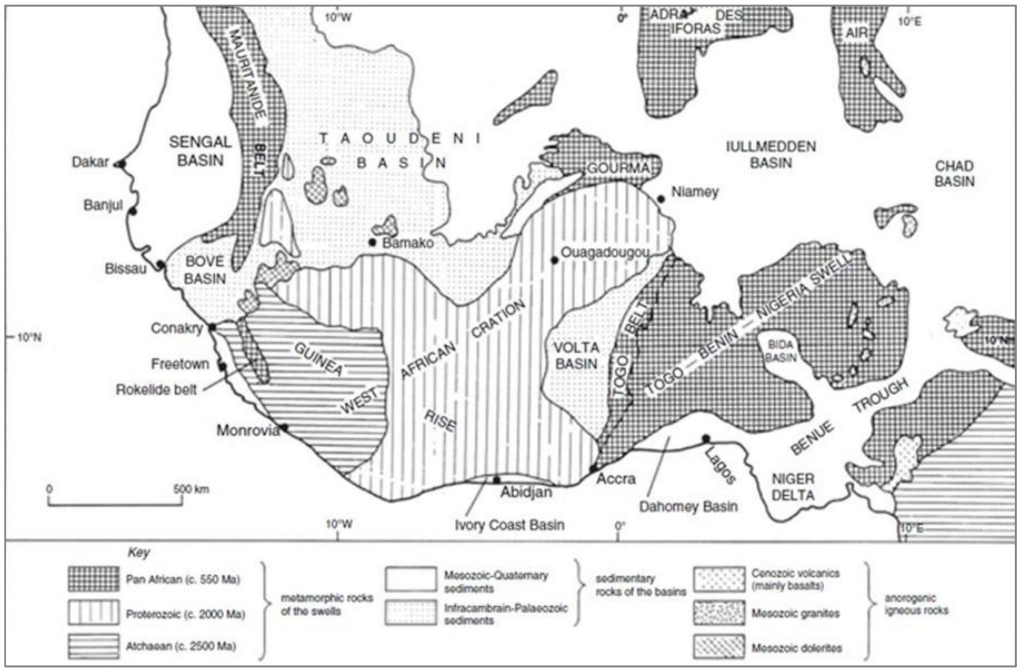

Fig. 2. Generalized geological map of Nigeria within the framework of the geology of West-Africa (Adapted from [14])

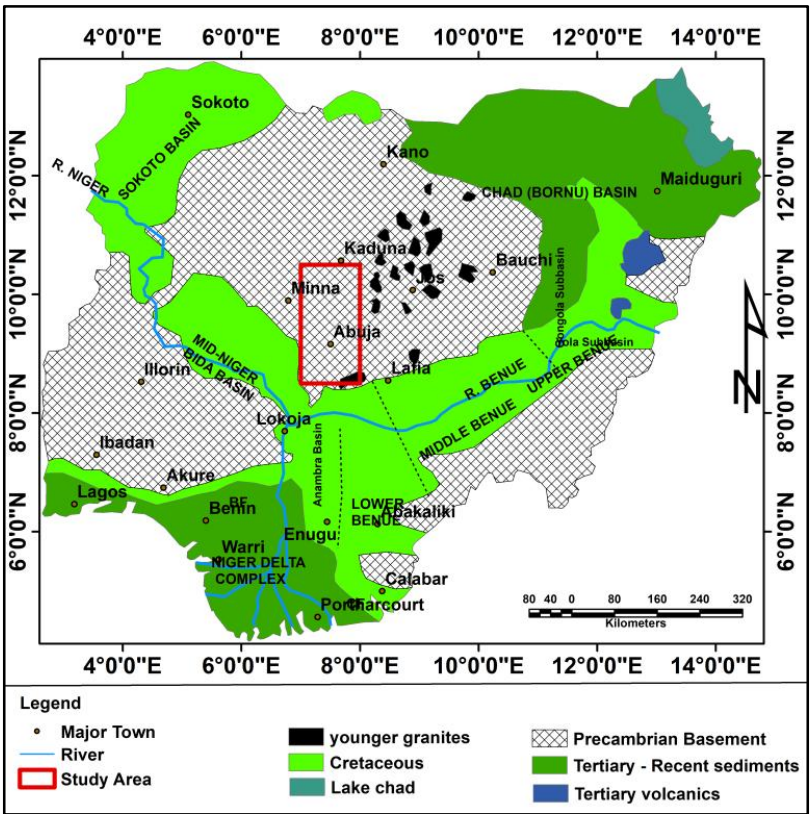

Fig. 3. Basement and sedimentary geology of Nigeria

The basement rocks are thought to be the result of at least four major orogenic cycles of deformation, metamorphism and remobilization corresponding to the Liberian (2,700 Ma), the Eburnean (2,000 Ma), the Kibaran (1,100 Ma), and the Pan-African cycles (600 Ma). Intense deformation and isoclinal folding accompanied by regional metamorphism characterized the first three stages, which was followed by extensive migmatization. A regional metamorphism, migmatization and widespread granitization and gneissification followed the Pan-African deformation, which produced syntectonic granites and homogenous gneisses [15].

The final stages of this last deformation were accompanied by late tectonic placement of granites and granodiorites, and associated contact metamorphism. Faulting and fracturing had marked the conclusion of the orogeny [16,17]. Four essential petro-lithological units can be differentiated within Nigeria's basement complex, namely: a. The Migmatite-Gneiss Complex (MGC) b. The Schist Belts (Metasedimentary rocks and Metavolcanics) c. The Older Granites (Pan African granitoids), and d. Undeformed acid and Basic Dykes.

The study area is exclusively Basement [8,9], with topography that varies from 116 m for low elevated areas to 986 m for very high elevated areas as obtained from analysis of Digital Elevation Model (DEM) Shuttle Radar Topography mission (SRTM) of the area (Fig. 4A). The area comprises of the following rock types: Migmatites which are the most predominant rock types with the schists (undifferentiated schist including phyllites that occur around north-western and eastern part of the study area and the Pelitic/Muscovite schists that occur around the south western part of the map). Other rock types are undifferentiated older granites, dolerites, porphyritic granite, granite and granite porphyry, granite gneiss, Medium to coarse grained biotite granite, Banded gneiss, migmatitic gneiss and biotite granites (Fig. 4B).

2. MATERIALS AND METHODS

The data used for this research consists of eight sheets (144 Kakuri, 145 Kajuru, 165 Bishini, 166 Kachia, 186 Abuja, 187 Gitata, 207 Kuje and 208 Keffi) aeromagnetic datasets. Fugro Airborne Surveys conducted the surveys for Nigerian Geological Survey Agency (NGSA) in 2009. The data were recorded for magnetic measurements at an interval of 0.1 s (~7.5 m). The airborne survey was flown perpendicular to the major geological trends in the area in the NW – SE direction, with a flight line spacing of 500 m, a terrain clearance of 80 m and a tie line spacing of 2000 m in the NE – SW direction. The resolution of the anomalies is immensely higher than conventional high-altitude airborne survey, based on the very short recording interval, lower survey flight height of 80 M, and narrower flight line spacing.

2.1 Methodology

The methods employed in this research include: Merging the eight (8) aeromagnetic data sheets that covers the area to form a single data base for the study to produce the Total Magnetic intensity (TMI) map using Oasis Montaj software. The gridded data were imported into Geosoft oasis Montaj version 8.4 and 6.4 environment where the data were save to data base and coordinate system was assigned to the grids imported for all grids data sheets that make up the study area after which it was exported as CSV file and the command prompt was used to join or merge the eight separate aeromagnetic data sheets into to one composite data sheet for the study area. This was done to avoid lines created by the knitting and blend function in oasis Montaj in some cases. Thereafter, the comma delimited (CSV) files were imported back into Geosoft environment where the magnetic data were gridded at 100 m grid spacing, using minimum curvature technique to produce the Total magnetic intensity map, the 100 m grid spacing, which is one-fifth of the survey flight line spacing, was used to avoid short-wavelength errors which may appear as lines perpendicular to the survey flight line [18]. The chosen grid cell size also satisfies the opinion of [19] that grid spacing should be between one-third and one-fifth of the survey flight line. The maps were processed using the Oasis Montaj software version 8.4 and version 6.4. The regional fields were removed by upward continuing the Total magnetic intensity data (TMI) grid to a height of 60 km and subtracting the resulting grid from the TMI grid in order to obtain the residual grid displays as a map given by 1:

$$Residual\ Field = TOTAL\ Field - Regional\ Field \quad (1)$$

The residual magnetic intensity (RMI) was reduced to the magnetic pole (RTP), using magnetic inclination of -4.68° and declination of -2.01° (IGRF of 2005) of the center point of the

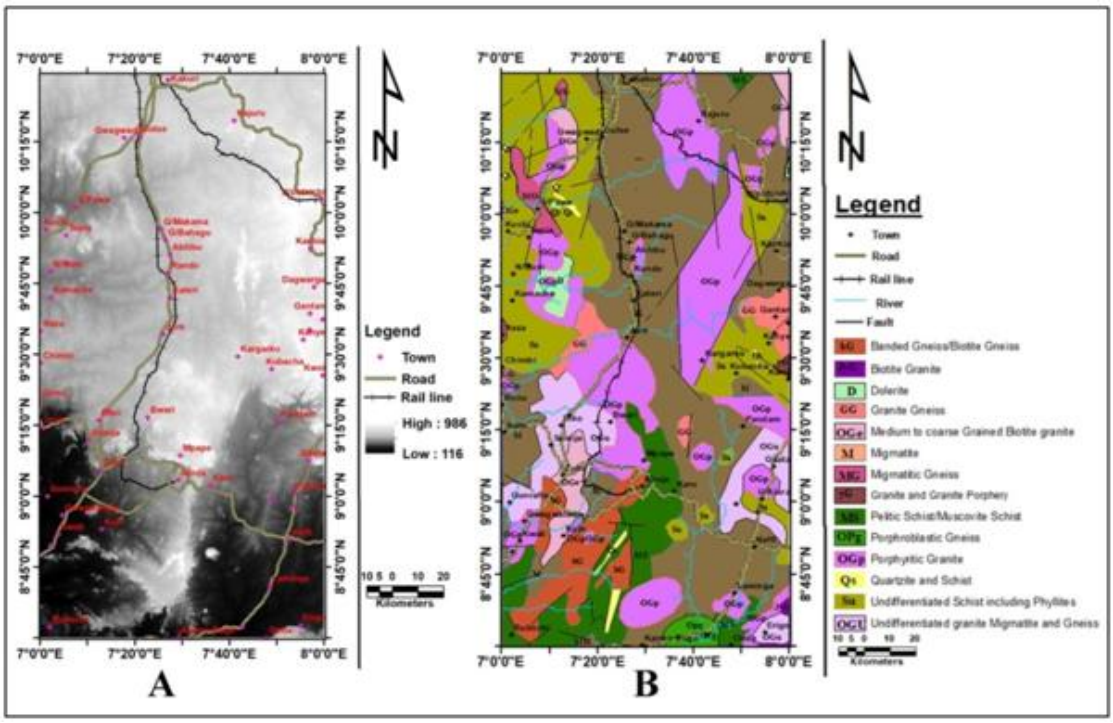

Fig. 4. A. SRTM DEM map showing topographic variations and B. Geologic map of the area

study area, so that anomalies observed would be directly positioned on their respective causative source bodies. The RMI was reduced to the magnetic pole, so that observed anomalies were vertically positioned directly on their respective source bodies.

Analytic Signal (AS) source edge mapping technique was applied on the residual magnetic intensity data reduced to pole (RTP) to delineate the magnetic source boundaries and magnetic discontinuities. The amplitude of analytic signal within the study area was achieved by calculating the square root of sun of squares of magnetic gradient in x, y and z directions using grid expression of Oasis Montaj. The tilt derivative which has proved to be very good in source edge mapping was applied to the RTP data with Euler deconvolution for depth, structure and geometry of the anomaly. Also, first vertical derivative transform as a useful interpretation tool in the determination of shallow seated fractures and faults by making the edges of shallow seated anomalies to become sharper or clearer, was applied to the RTP data to delineate near surface structures (lineaments) and the Rose diagram of the structures delineated from all the source edge mapping technique maps was produced. Also, the structures (Lineaments) delineated were used to produce structural density map. Second vertical derivative (SVD) method was also applied to the RTP data of the area which aided in structural mapping and delineation of anomaly or source boundaries and possible mineralization zones.

2.2 Reduction to Magnetic Pole

The aim of reduction to the pole is to take an observed total magnetic field and produce a map that would have resulted had an area been surveyed at the magnetic pole. Reduction to the pole is the process of converting the magnetic field from magnetic latitude where the Earth's field is inclined, to the field at a magnetic pole, where the inducing field is vertical [20]. When the Earth's field is inclined, magnetic anomalies due to induction have forms that are asymmetrically related to their sources, but when the inducing field is vertical, the induced anomalies are directly over their sources [21]. Assuming that all the observed magnetic fields of a study area are due to induced magnetic effects, pole reduction can be calculated in the frequency domain as in equation (2) [22].

$$L(\Theta) = \frac{1}{[\sin(I)+i\cos(I)\ \cos(D-\Theta)]^2} \quad (2)$$

where,

θ is the wavenumber direction
I is the magnetic inclination, and
D is the magnetic declination

2.3 Upward Continuation

Upward continuation attenuates the anomalies of shallow features and relatively enhances the anomalies of deeper sources making it applicable for regional-residual separation [23]. When the relatively deeper sources are subtracted from the total field, the resultant is the shallow features known as the residual field [24]. The frequency response of upward continuation filter is given as

$$F_u(u,v,h) = e^{-2\pi h}(u^2 + v^2)^{\frac{1}{2}} \quad (3)$$

where h is the height to which the field is continued and "u" and "v" are equivalent of x and y coordinates in the frequency domain. Upward continuation may be applied to suppress the effects of small scale features near the surface [24]. It is also used to reduce topographic effects. For a total field F(x, y, 0).

$$F(x,y,-h) = \frac{h}{2\pi}\iint \frac{F(x,y,0)\partial x\partial y}{(x-x^i)^2+(y-y^i)^2+h^2} \quad (4)$$

Equation 4 is the upward continuation equation that allows us to calculate magnetization anywhere in the free space from the knowledge of its values over the surface. The left side is the total field at the point P(x, y, -h) above the surface F(x, y, 0) on which it is known.

2.4 Analytic Signal

Analytic signal otherwise called total gradient is a popular gradient enhancement, which is related to magnetic fields by the derivatives. [25] showed that the amplitude of the analytic signal can be derived from the three orthogonal gradient of the total magnetic field using the expression:

$$|AS(X,Y)| = \sqrt{\left(\frac{\delta T}{\delta x}\right)^2 + \left(\frac{\partial T}{\partial y}\right)^2 + \left(\frac{\delta T}{\delta z}\right)^2} \quad (5)$$

where AS is the amplitude of the analytic signal at (x, y) and T is the observed magnetic anomaly at (x, y). This function is extremely interesting in the context of interpretation, in that it is completely independent of the direction of the magnetization and the Earth's magnetic field. This means that all bodies with the same geometry have the same analytic signal. The analytic signal displays maxima over the source body edges even when the direction of the magnetization is not vertical [25].

2.5 Tilt Derivative

The tilt angle or derivative ratio (TDR) is defined as the arctangent of the ratio of vertical derivative to total horizontal derivative of the magnetic field M [26-29].

$$TDR = \tan^{-1}\left[\frac{\partial M/\partial z}{\sqrt{(\partial M/\partial x)^2+(\partial M/\partial y)}}\right] \quad (6)$$

In equation 6 above, $\partial M/\partial x, \partial M/\partial y$, and $\partial M/\partial z$ are first-order derivatives of the magnetic field in the x, y and z directions. Base on [29], the TDR values vary between −π/2 and +π/2. The TDR crosses through zero at or near the edge of a vertical source and is negative outside the source region. Also, [30-33] have proved that the half-distance between ±π/4 contours gives an approximation of the source depth for vertical contacts. The distance between zero and +π/4 or −π/4 contour obtained from the TDR represent the depth to the top of the vertical contact.

2.6 Euler Deconvolution

According to [34], Euler deconvolution is both a border and a depth estimator. It extracts data from grids using the homogeneity relationship shown by [35]. This relationship can be written in the following form:

$$(x-x_0)\frac{\delta T}{\delta x} + (y-y_0)\frac{\delta T}{\delta y} + (z-z_0)\frac{\delta T}{\delta z} = N(B-T) \quad (7)$$

where (x_0, y_0, z_0) is the position of a magnetic source whose total field T is detected at (x, y, z). B is the regional field value, and the degree of homogeneity interpreted as the structural index (SI) which is a measure of the rate of change at field distance is represented by N, and this structural index was chosen based on prior knowledge of the source geometry. [34] also put forward that, structural index (SI) ranges from zero (0) to three (3) for distinct bodies (N= 0 for contacts, 1 for sill/dyke/fault, 2 for pipe/horizontal bodies, and 3 for spherical bodies).

2.7 First Vertical Derivatives

This technique accentuates short wavelength and is relatively insensitive to noise. Mostly used

for delineating near surface lineaments and contacts [36]. The First vertical derivative has shown to be a useful technique in the processing of magnetic data; it is a filtering technique that is equivalent to enhancing shallow sources and suppressing deeper sources [37]. The transform is a useful interpretation tool in the determination of shallow seated fractures and faults by making the edges of shallow seated anomalies become sharper or clearer. The mathematical expression involved is given by equation 8:

$$VD = \frac{\partial T}{\partial Z} \quad (8)$$

Where VD is equal to the vertical derivative while $\frac{\partial T}{\partial Z}$ is the magnetic field in Z direction. The first vertical derivative filter does the removal of the long wavelength properties of magnetic responses and most importantly enhances the quality of closely spaced and superposed responses [38].

2.8 Second vertical Derivatives (SVD)

While the second vertical derivative is the vertical gradient of the first vertical derivative and has even more resolving power than the first vertical derivative, but its application requires high quality data as its greater enhancement of high frequencies results in greater enhancement of noise. Higher orders of derivatives are virtually never used to produce interpretation products [39]. [40] showed that the second vertical derivative is zero and swiftly changes sign over at a point vertically over a contact. In the analysis of magnetic data, second vertical derivatives are used to delineate the plain-view boundaries of intra-basement anomaly sources and are also found to be useful for enhancing magnetic anomalies [41]. The zero-point (of the second vertical derivative) of the image map shows the spatial positions of the magnetic source edges which in turn outline anomalous areas.

3. RESULTS AND DISCUSSION

3.1 Total Magnetic Intensity (TMI) and Residual Magnetic Intensity (RMI)

The total magnetic intensity map (Fig. 5A) reveals variation in magnetic signatures within the study area from south to north and from the east to west. Within the study area, amplitudes of the magnetic anomalies of the rocks depend on magnetization which subsequently corresponds to the magnetic susceptibility of these rocks as formations at low magnetic latitude (Close to the Earth equator) areas are magnetized in the same direction as (parallel to) the magnetic field of the Earth, therefore, it is possible for some high magnetic susceptible regions to show low magnetic values while less magnetic susceptible areas also show high magnetic values within the study area. The magnetic intensity values within the area ranges from 32949.581 nT minimum to 33117.780 nT maximum with total number of 2,428,540 data points. The area is marked by both magnetic lows and high closures which could be attributed to difference in the lithology of the rocks, difference in the magnetic susceptibility of the rocks within the area, variation in depth to magnetic source within the study area and degree of strike. Several Magnetic highs and lows were observed as closures on (Fig. 5A). Circular to near circular closures are probably caused by circular to near circular ore bodies or intrusions while elongated closures represent almost linear anomalies caused by long ore bodies or dykes. At the southern part of the map across the study area from latitude 9°15^1 in the east across the map and longitude 8°45^1 in the west down to the end of the map is dominated by high magnetic closures having magnetic trend of NE-SW. The high magnetic signatures around south western portion of the study area trending NE-SW coincide with metasediments (Pelitic Schist and Muscovite Schist), Banded gneiss/biotite granite and porphyritic granite. The high magnetic anomalies that occur around south eastern part of the area coincide with the older granitoids (Porphyritic granite, undifferentiated granite/Migmatite gneiss). The central portion of the map (Fig. 5A), within north and south of latitude 9°30^1 and longitude 7°30^1 to the western end of the study area, there is an alternating occurrence of short wavelength anomalies which coincide with basement that may be exposed to the surface and long wavelength anomalies that are probably basement with thick sedimentary cover. The magnetic closures within this area showed almost E-W magnetic trends and this coincided with undifferentiated granite/ Migmatite/gneiss and pelitic schist /muscovite schist. At the extreme north of the study area between longitude 7°20^1 E and longitude 7°40^1 E (Fig. 5A), anomaly trend is NW-SE. Also, the low magnetic intensity value observed within the magnetic highs with east to west trends in the central portion of the map towards the western end suggests the presence of deep-seated fault zone which trends in the same direction as the

observed anomaly (Fig. 5A) while Fig. 5B represent the residual magnetic intensity (RMI) map of the study area. The map when compared to the TMI map shows magnetic high around north-eastern portion of the area. This is attributed to shielding effects of regional anomaly that has now been removed.

3.2 Residual Magnetic Intensity (RMI) Reduced To Pole (RTP)

The RMI data was reduced to the pole prior further processing to correct the effect of latitude, to realign the anomalies and have their peaks symmetrically centered over their corresponding sources because the study area is very close to the equator. This was achieved using geomagnetic inclination of -4.68° and geomagnetic declination of -2.01° of the central point of the study area to get the actual position of the magnetic anomalies without losing any geophysical meaning (Fig. 6A). The RTP map (Fig. 6A) when compared to the RMI (Fig. 5B) map shows variation in their magnetic intensities. The RTP map have magnetic intensities that varies from -50.300 nT minimum 138.550 nT maximum compared to RMI map where the magnetic intensity values within the area ranges from -78.272 nT minimum to 150.240 nT. There are observed similarities between the two maps with regard to the displayed anomaly in terms of anomalies trends, especially their symmetry, strike, extension, and width. The differences between the two maps are so obvious especially the reverse in magnetic intensity where it was high on RMI map is now showing low on the RTP map. As pointed out by [37], portions on the maps (Fig. 6A and 6B) having alternating occurrence of magnetic high and lows could be attributed to faults/highly fractured nature of the area as oxidation in fractured zones during weathering processes commonly leads to the destruction of magnetite which often allows such zones to be picked out on anomaly maps as narrow zones with markedly less magnetic variation than in the surrounding rocks.

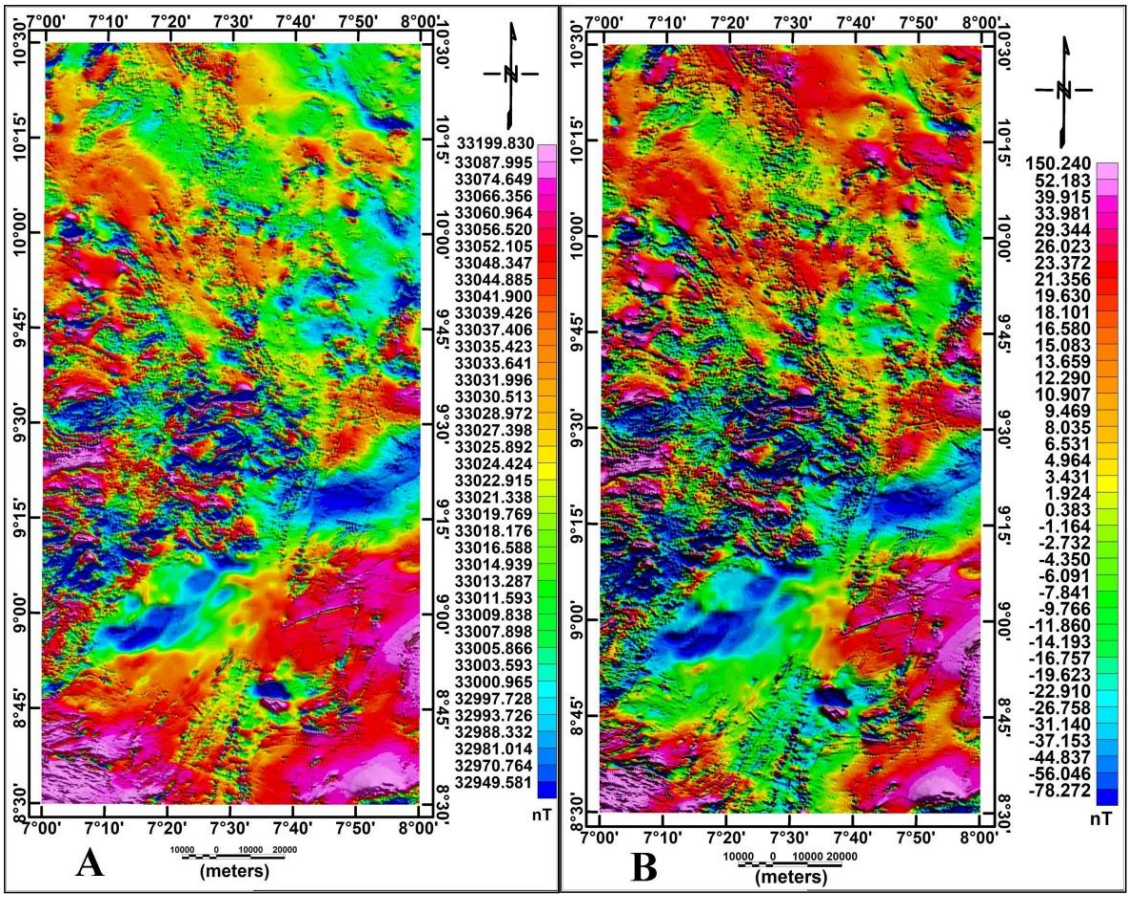

Fig. 5. A. TMI map and B. RMI map

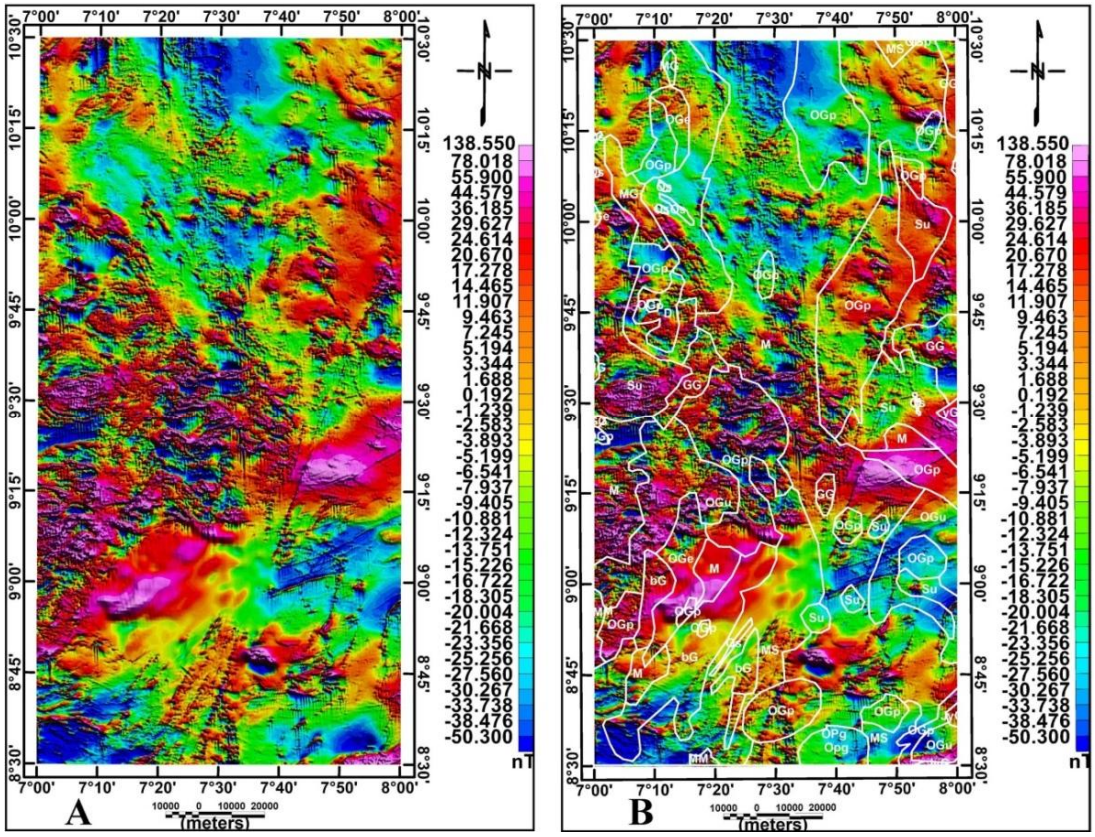

Fig. 6. A. RMI reduced to pole map and B. RTP map with geology of the area

(M = Migmatites, Su = Undifferentiated schist including phyllites, MS =Pelitic/Muscovite schists, OGu= Undifferentiated older granites, D = dolerites, OGp = porphyritic granite, yG = granite and granite porphyry, GG= granite gneiss, OGe = Medium to coarse grained biotite granite, bG= Banded gneiss, MG = migmatitic gneiss and JyG = Biotite granites)

This could also be attributed to the effect of metasomatic alteration of magnetite and /or hydrous Fe-oxide developed in fractures that lead to the decrease in the magnetic susceptibility of the host rocks [42]. Within the central part of the map (Fig. 6B) to the west where all the rock type are characterize by both magnetic high and low, the magnetic high is attributed to large scale basic magmatic intrusions of high magnetite contents that affected the rocks while the magnetic lows are attributed to effect of metasomatic alteration of magnetite and /or oxidation during weathering processes that leads to destruction of magnetite.

3.3 Analytic Signal Map (AS), Tilt Derivative (TDR) and Euler Deconvolution

The analytic signal map is good in locating contacts and sheet like structures by forming maxima around the edges of magnetic sources. The analytic signal map (Fig. 7A) has accentuated the variation in the magnetization of the magnetic sources in the study area and highlights discontinuities and anomaly texture. These structures are observed around the central portion of the area and also span towards the western end of the map.

The analytic signal amplitude maximizes over the edge of the magnetic structures as a result, the high magnetic anomalies zones are associated with highly rich ferromagnesian-bearing rocks with minor felsic minerals [24]. The analytic signal map has amplitudes that range from 0.003 to 0.256. The map could be said to have exhibited three different magnetic zones in this area of study based on the amplitude of the anomalies within this area. Low to fairly low magnetic zone (LM) with an amplitude range of 0.003 to 0.009 are areas associated with highly weathered rocks and areas with thick cover of sediments, metasediments, and granite because

these rocks contain more than 60 to 70% quartz. The moderate magnetic zone (MM) with amplitude 0.009 to 0.106 is associated with granite – gneiss as these rocks contain high ferromagnesian with low amount of felsic minerals. Rocks with largest amplitudes have high content of felsic minerals. The highest amplitude areas above 0.106 could represent areas of later tectonic activities where magma intruded into the pre-existing rocks and solidify in the fractures, faults, and joints left by earlier tectonic activities. These are areas within the central portion of the map towards the western edge from latitude 8°30[1] N to latitude 10°N (Fig. 7A), while Fig. 7B represents the tilt derivative map of the area that was generated from RTP data of residual magnetic data of parts of north central Nigeria. The map indicates that the TDR anomaly map could be used for recognition of the horizontal location and extent of edges of various sources assuming vertical contact model. The zero contours estimate the horizontal location of abrupt lateral changes in the subsurface features. Short wavelengths have been highlighted on the TDR map. Another advantage of the TDR map Fig. 7B is that it has equalizes the amplitudes of the shorts and long-wavelength potential field anomalies and the TDR zero contours have delineated the spatial location of the magnetic source edges within the area.

In the present study, the standard Euler Deconvolution method has been applied to the RMI reduced to the pole (RTP) grid data of the study area, using structure index of one (SI=1) to delineate the depth and location of the basement rock contact and/or faults with dykes. The obtained Euler solution maps (Fig. 8A) and (Fig. 8B) overlaid by (Fig. 8A) show depth solutions that were grouped into four, those below 150 m, 150 m to 300 m, those between 300 m to 450 m and those above 450 m respectively. The Euler solution maps have assisted in drawing the boundaries of causative bodies and trends of structures revealed in the study area at the specified depths. Faults/structural trends coincided with the edges delineated from tilt derivative map as (Fig. 8A) is overlaid on (Fig. 8B).

3.4 First Vertical Derivative Map

The color and grey images of the first vertical derivative (Fig. 9A and 9B) enhanced the image by showing major structural and lithological detail which were not obvious in TMI, RMI map and RTP maps (Fig. 5A, 5B and 6A). The structures extracted from FVD and analytic signal maps (Fig. 9B and Fig. 7A) were overlaid on Euler solution map with structural index of one (SI=1) to ascertain depth of these structures delineated (Fig. 10) where most of the structures delineated are found between depths of 150 m to 500 m. Also, the spatial distribution of lineaments extracted from aeromagnetic images according to their length and orientation to help illustrate the faults in the study area and to obtain more details on the distribution and existence of the lineaments. Structures (Lineaments) were analysed and a common technique called rose diagram was applied for this purpose. For structures such as joints or fault planes reflecting the angular relationships of geological map data, Rose Diagram was used to show graphically the different tendencies. Fig. 11A is a Rose Diagram representation of the regional strike of the delineated lineament from aeromagnetic data by using a polar plot where the distance from the center of the plot is proportional to the sum of the line lengths in that orientation. Structural lineament orientation or azimuth direction on the structural lineament map (Fig. 9B) were measured using (Arc Map version 10.5) and plotted as a rose diagram using rockworks software. The rose (azimuth-frequency) diagram (Fig. 11A) depicted most of the lineament extracted trends majorly ENE-WSW direction followed by WNW- ESE, and minor NE-SW, NW-SE, NNE- SSW and NNW-SSE. This is in confirmation with "[43] that studied the Benue Trough's tectonic framework and that of parts of the adjoining Nigerian basement complex using aeromagnetic maps, delineating NE-SW and ENE-WSW directions as being the dominant aeromagnetic lineament trends" followed by WNW-ESE with minor NE-SW, NNE-SSW and NNW-SSE Pan-African trends.

Lineament density analysis (Fig. 11B) depicted the central portion of the map to be very dense with structures. These are areas suspected for possible mineralization because of presence of more of the structures within these areas. Two of the four transatlantic faults that pass through Nigeria through the Atlantic Ocean, the ST Paul's and the Romanche both appear to pass through the study area and were delineated on the FVD map (Fig. 12) as stated by [43] that these aeromagnetic lineaments depicted a possible continental continuation of the four Atlantic fracture zones (St Paul's, Romanche, Chain and Charcot) abutting the West African coast into the Nigerian basement complex.

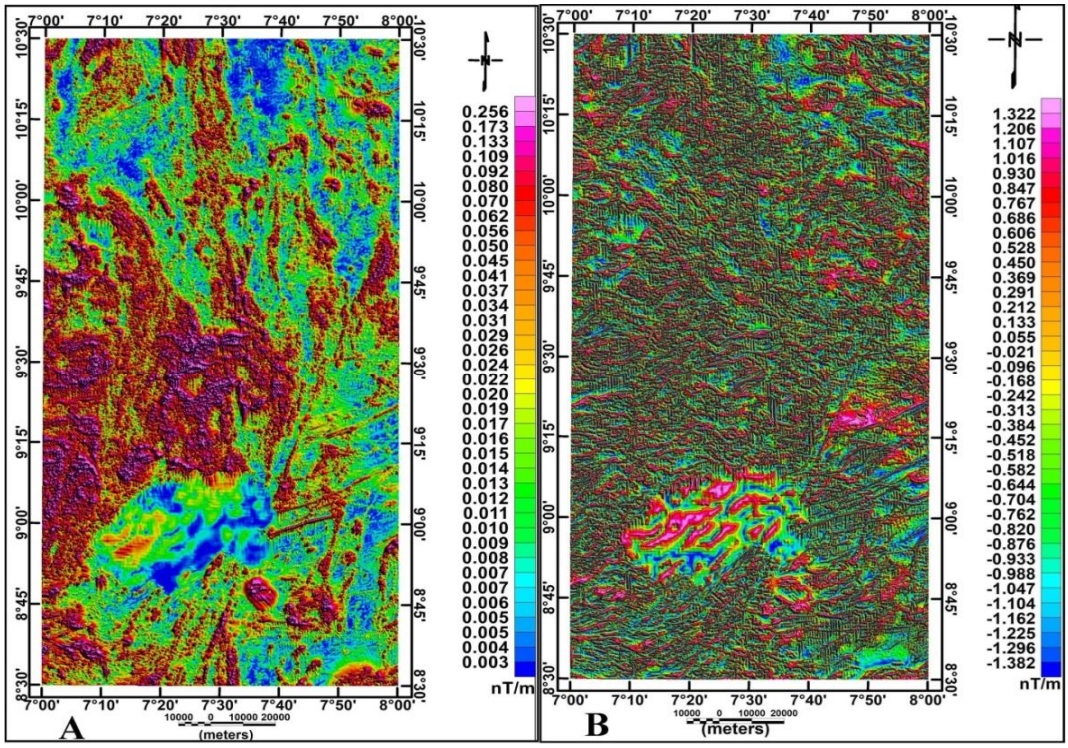

Fig. 7. A. Analytic signal map (AS) and B. Tilt derivative map (TDR)

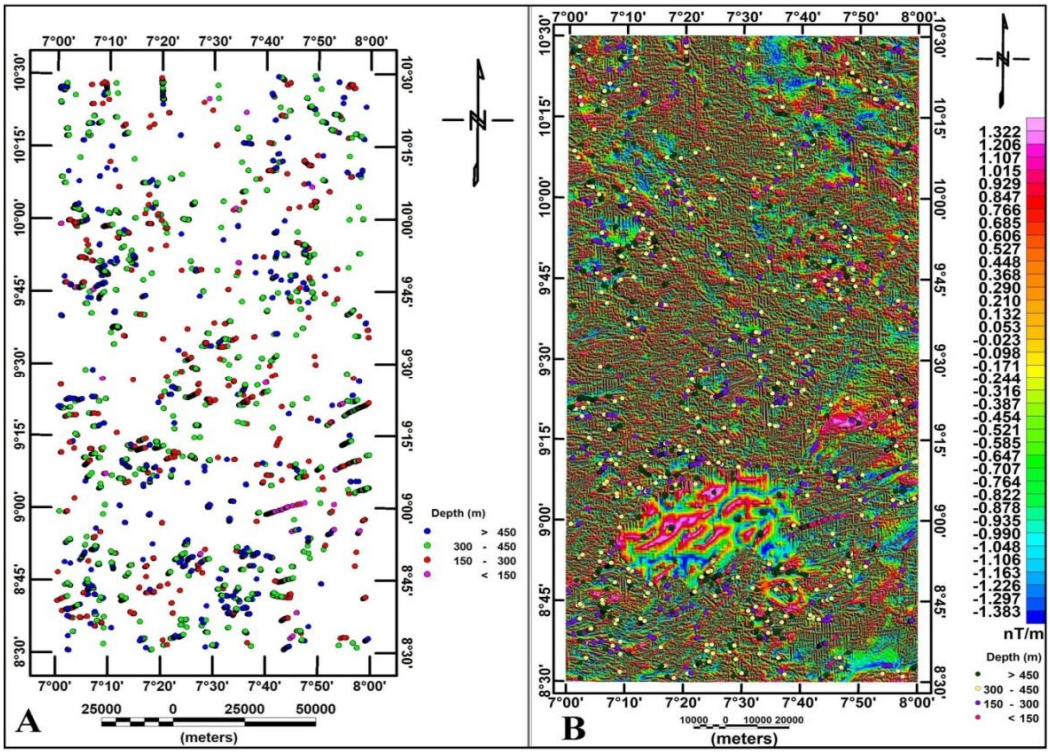

Fig. 8. A. Euler solutions with structural index (SI=1) for sills/dykes/faults
B. Tilt derivative map with euler solutions

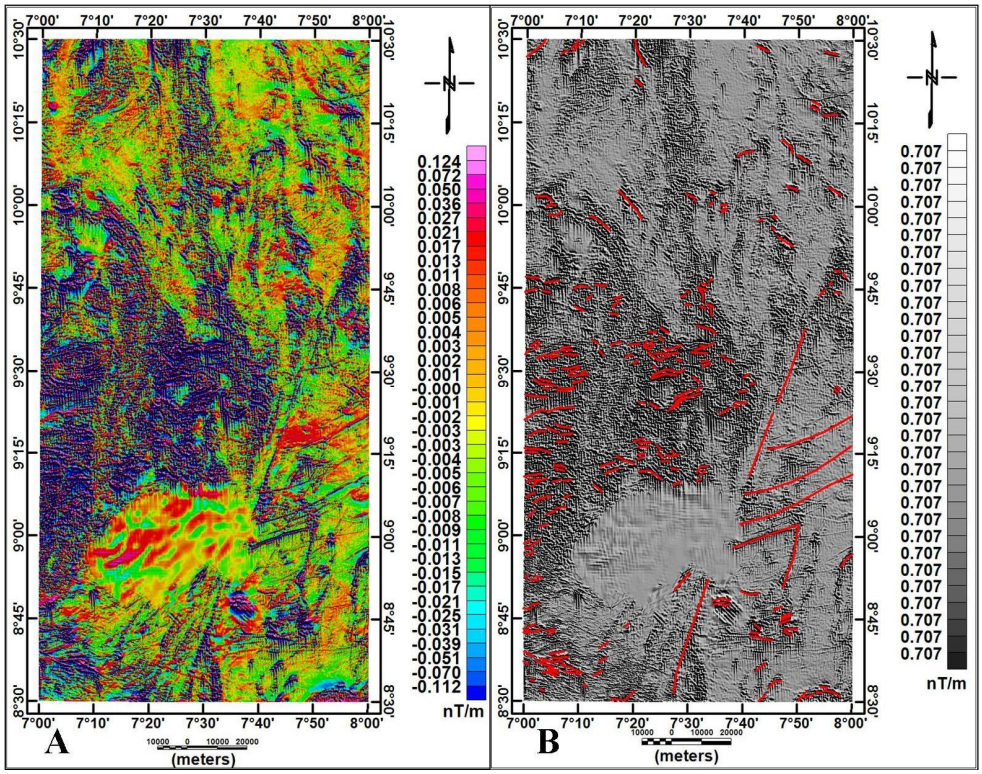

Fig. 9. A. FVD color map and B. FVD grey shaded map with structures

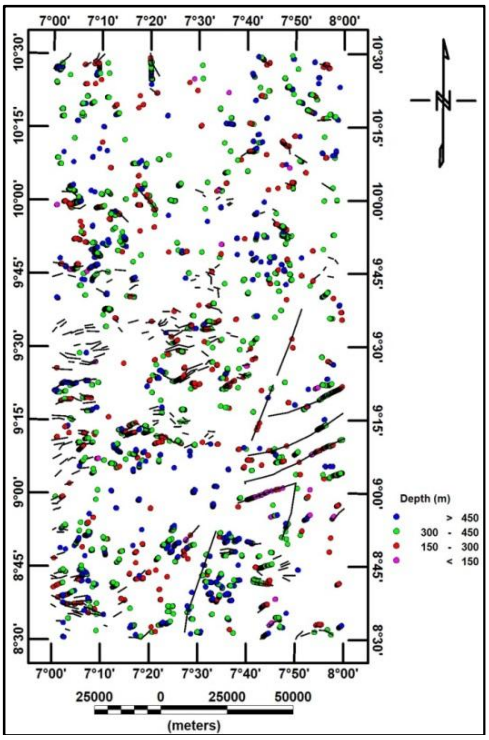

Fig. 10. FVD structures with Euler solution structural index of one (SI=1)

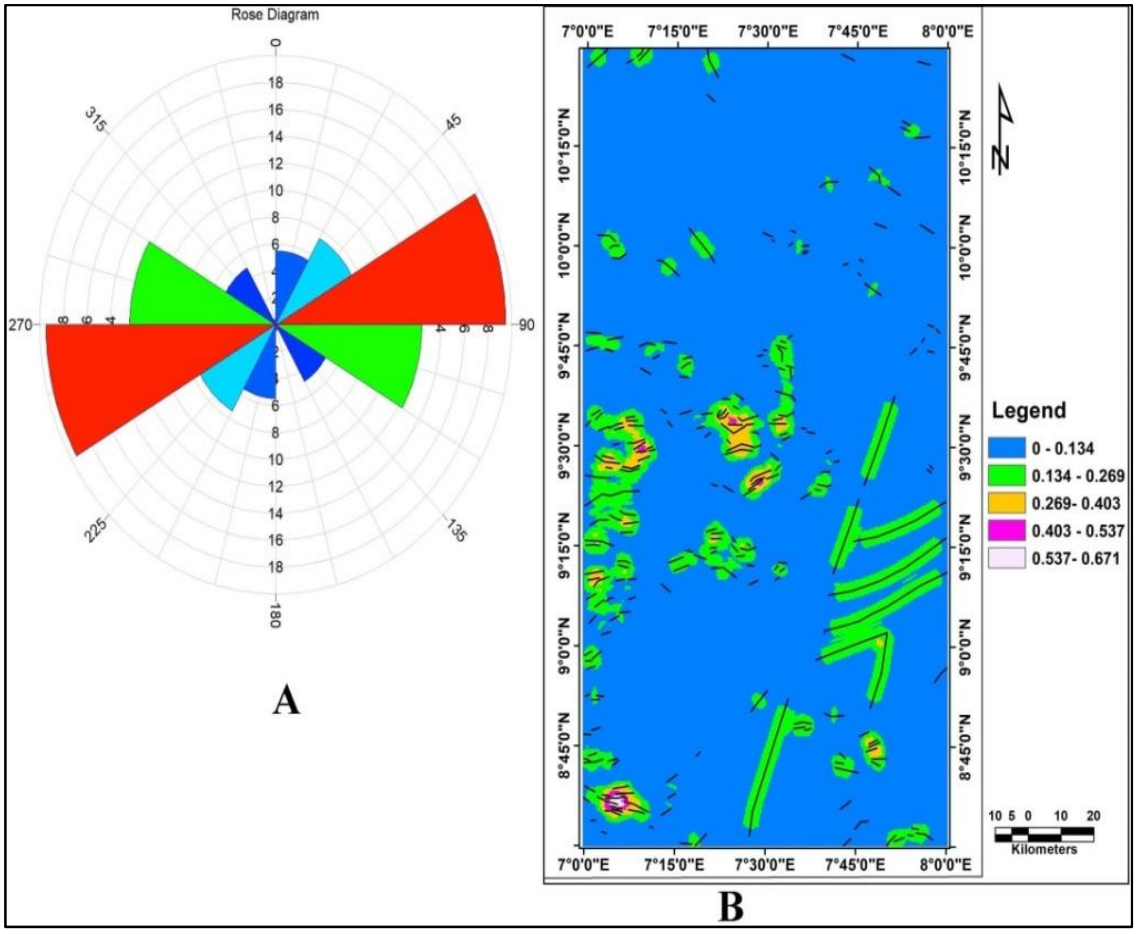

Fig. 11. A. Rose diagram, B. Structural density map and

3.5 Second Vertical Derivative (SVD)

The second vertical derivative (SVD) map produced (Fig. 13A) has enhanced subtle anomalies while reducing regional trends, accentuated anomaly boundaries of near surface effects and has defined the edges of the causative bodies within the study area and amplified structure/lineament/fault trends (Fig. 13B) with longest fault trending north-east to south-west suspected to be a paleostructure (Fig. 12). On the second vertical derivative map, the boundaries of the shallow anomalies have been clearly revealed and this has made it possible to delineate possible mineralization zones in polygonal shapes, most of which falls within the western half of the study area. The second vertical derivative map can be correlated with analytic signal map (Fig. 7A).

The structures delineated using first vertical derivative technique (Fig. 9B) and possible mineralization zones delineated using second vertical derivative map (Fig. 13B) were over laid on the geologic map of the area (Fig. 4B) to infer possible mineral occurrence. A detailed look at the map (Fig. 14) based on the geology of the areas delineated from SVD map revealed the western edge of the study area delineated (mineralization) zones from the north to the middle of the map to be undifferentiated schist including phyllites and quartzite and schists with some parts that fall on the porphyritic granites. Mineral occurrence within these zones may be Gold (AU) as most of the Gold occurrences in Nigeria are within the schist belts as the schist at that location are continuation and extension of the schists in the north within Birnin Gwari which is already known to be rich in Gold. The Gold here could occur as both placer and primary veins [45,8]. The veins are hosted by quartzite, schists and phyllites (Fig. 14). For areas within the central portion, minerals that can possibly be found there are Ilmenite, Bismuth,

Cassiterite (Tin Ore), Gemstone, Tantalite and Iron Ore with the following possible style of mineralization:

i. Pegmatite pods with quartz, topaz, beryl and feldspar; ii. Pervasive metasomatic disseminated mineralization with Columbite or pyrochlore ± Cassiterite; iii. prejoint and post joint pegmatitic pods and lenses with albite or microcline, genthelvite, uraninite, Columbite and thorite; iv. quartz rafts, stockworks, sheeted veins and altered wall rock with Cassiterite, wolframite and sulphides; v. fissure-filling veins or lodes with Cassiterite, wolframite and sulphides; vi. Irregularly shaped replacement bodies with Cassiterite and sulphides; vii. Quartz veins with wolframite or scheelite, bismuth minerals, sometimes abundant Cassiterite and/or sulphides and viii. Mineralized ring-dyke with Cassiterite and sulphides [8].

Also, a closer look at the Map (Fig. 14) revealed the pelitic schist /muscovite around the central portion and south western portion of the map to be mineralized as such, Gold is also expected to be found within the area in form of veins and in lead-Sulphides mineralization.

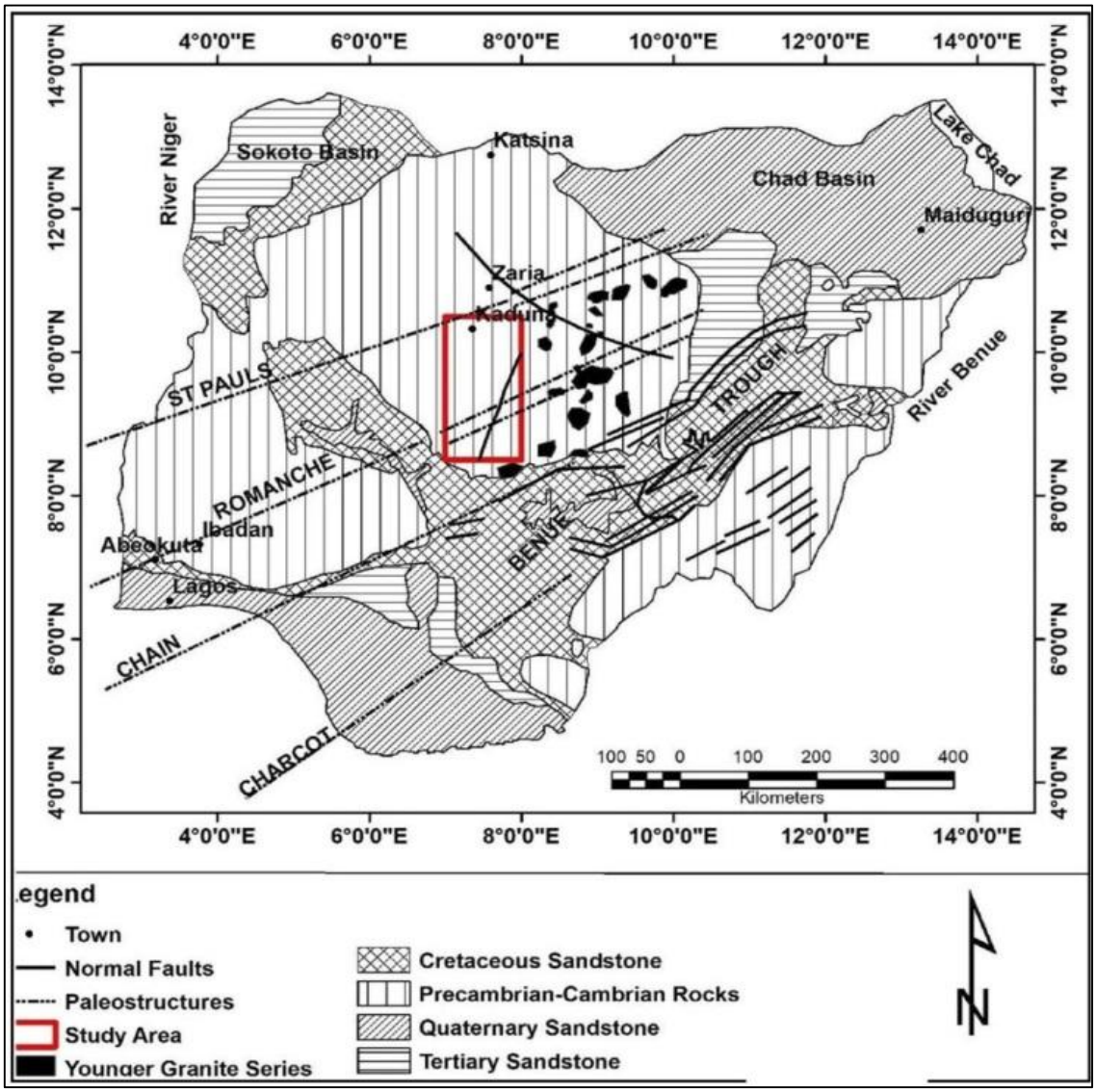

Fig. 12. Transatlantic fault map modified from [44]

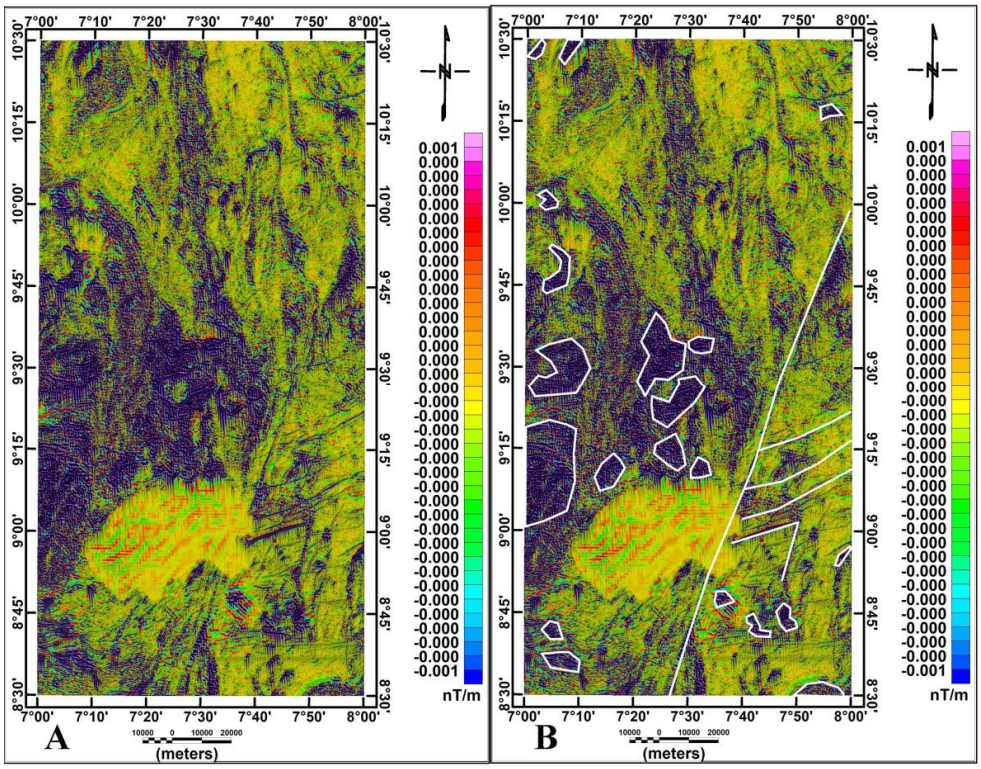

Fig. 13. A. SVD map and B. SVD map with delineated mineralization zones

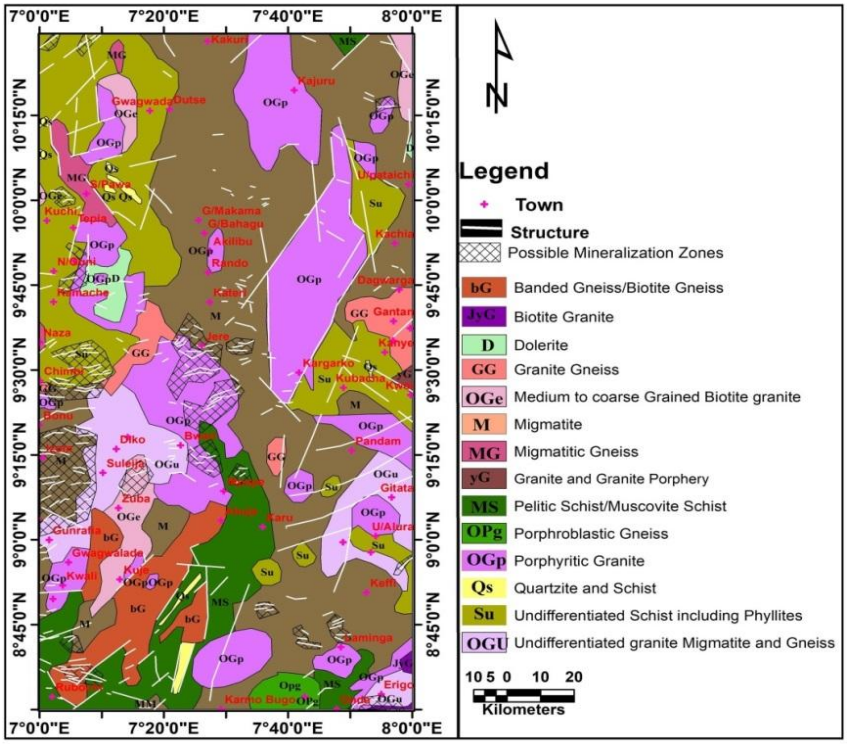

Fig. 14. Geologic maps with delineated mineral occurrence zones

4. CONCLUSIONS

Aeromagnetic data sets were analyzed using different filters to enhance geological features of interest within the study area. Analysis carried out using the TMI, RMI, RTP and upward continuation filters were helpful in identifying different magnetic anomalies within the study area. From the analytic signal map, three magnetic zones were delineated. These are: low to relatively low magnetic zone (LM) with amplitude range from 0.003 to 0.009, moderate magnetic zone (MM) with amplitude 0.009 to 0.106 and those with high amplitudes above 0.106 which are products of later magmatic intrusions into host rocks with fractures, faults and joints. Areas of high analytic signal are predominant within the central portion of the study area and span towards the western end of the map. The tilt derivative map helped in delineation of horizontal location and extent of edges of various causative sources while Euler deconvolution helps in the determination of boundary, depth and geometry of the structures. The first vertical derivative map (FVD) aided in manual structural delineation within the study area, while the second vertical derivative (SVD) map also helped in delineating possible mineralization zones that are pronounced within the study area, around portion with rocks of high analytic signal. Structural analysis of aeromagnetic data as delineated from all the source edge enhancement techniques used reveals five tectonic structural trends in the directions ENE-WSW, NE-SW, NNE-SSW, NNW-SSE and WNW-ESE with ENE-WSW being the predominant or major structural trend.

COMPETING INTERESTS

Authors have declared that no competing interests exist.

REFERENCES

1. Paterson NR, Reeves CV. Applications of gravity and magnetic surveys: The state-of-the-art in 1985. Geophysics. 1985;50: 2558-94.
2. Ajakaiye DE, Hall DH, Ashiekaa JA, Udensi EE. Magnetic anomalies in the Nigerian continental mass based on aeromagnetic surveys. Tectonophysics. 1991;192(1):211-230.
3. Amigun JO, Anu AL. Integrated geophysical mapping of structures beneath Ijero – Aramoko Area, Southwestern Nigeria: Implications for control of mineralization. Acta Geologica Sinica. 2013;87:708.
4. Daniel E, Jimoh R, Lawal K. Delineation of gold mineral potential zone using high resolution aeromagnetic data over part of Kano State, Nigeria. Journal of Geology and Geophysics. 2019;8:464.
   DOI: 10.35248/2381-8719.464
5. Ayuba RA, Nur A. Analysis of high resolution aeromagnetic data and satellite imagery for mineral potential over parts of Nasarawa and environs. North-Central Nigeria. International Journal of Scientific and Technology Research. 2018;7(6).
6. Jamaluddeen SS, Aku MO, Saleh M, Bunawa AA, Sharafa SB. A reconnaisance study to delineate the potential mineral zones around the schist belt areas of Kano State, Nigeria using airborne magnetic data. Journal of Geology and Mining Research. 2018;11(2):14-21.
7. Anudu GK, Onuba LN, Onwuemesi AG, Ikpokonte AE. Analysis of aeromagnetic data over Wamba and its adjoining areas in north-central Nigeria. Earth Science Research Journal. 2012;16(1):25–33.
8. Obaje NG. Geology and mineral resources of Nigeria, Berlin: Springer-Verlag, Heidelberg. 2009;221.
9. NGSA. Geology and structural lineament map of Nigeria; 2006.
10. Hodges G, Amine D. Exploration for gold deposits with airborne geophysics. KEGS PDAC Symposium; 2010.
11. Black R. Precambrian of West Africa. Episodes. 1980;4:3–8.
12. Dada SS. Proterozoic evolution of Nigeria. In: Oshi O (ed) The basement complex of Nigeria and its mineral resources (A Tribute to Prof. M. A. O. Rahaman). Akin Jinad & Co. Ibadan. 2006;29–44.
13. Burke KC, Dewey JF. Orogeny in Africa. In: Dessauvagie TFJ, Whiteman AJ (eds), African geology. University of Ibadan Press, Ibadan. 1972;583–608.
14. Wright JB. Geology and mineral resources of West Africa. George Allen and Unwin, London. 1985;187.
15. Abaa SI. The structure and petrography of alkaline rocks of the Mada Younger Granite Complex, Nigeria. Journal of African Earth Science. 1983;3:107–113.

16. Olayinka AI. Geophysical siting of boreholes in crystalline basement areas of Africa Journal of African Earth Science. 1992;14:197–207.
17. Gandu AH, Ojo SB, Ajakaiye DE. A gravity study of the Precambrian rocks in the Malumfashi area of Kaduna State, Nigeria. Tectonophysics. 1986;126:181–194.
18. Anudu GK, Stephenson RA, Macdonald D. M. Using high resolution aeromagnetic data to recognize and map intra-sedimentary volcanic rocks and geological structures across the Cretaceous middle Benue Trough, Nigeria. Elsevier Journal of African Earth Science. 2014;99:625–636.
19. Dentith M. Magnetic methods, airborne. In: Gupta HS (ed) Encyclopedia of solid earth geophysics. Springer, Dordrecht. 2011;1: 761–766
20. Luo Y, Xue DJ, Wang M. Reduction to the pole at the geomagnetic equator. Chinese Journal of Geophysics. 2010;53(6):1082-1089.
21. Milligan PR, Gunn PJ. Enhancement and presentation of airborne geophysical data. AGSO Journal of Australian Geology and Geophysics. 1997;17(2):64–774.
22. Grant FS, Dodds J. MAGMAP FFT processing system development notes', Paterson Grant and Watson Limited; 1972.
23. Reynolds JM. An introduction to Applied and Environmental Geophysics, John Wiley and Ltd. Bans Lane, Chichester. 1997;124-13.
24. Telford WM, Geldart LP, Sherriff RE, Keys DA. Applied geophysics. Cambridge: Cambridge University Press. 1990;860.
25. Roest W, Verhoef J, Pilkington M. Magnetic interpretaion using 3-D analytic signal. Geophysics. 1992;57:116-125.
26. Rajaram M. What's new in interpretation of magnetic data? Geohorizons. 2009;50.
27. Salem A, Williams S, Fairhead JD, Smith R, Ravat DJ. Interpretation of magnetic data using tilt-angl derivatives. Geophysics. 2008;73:L1–L10.
28. Verduzco B, Fairhead JD, Green CM, MacKenzie C. The meter reader – new insights into magnetic derivatives for structural mapping. The Leading Edge. 2004;23:116–119.
29. Miller HG, Singh V. Potential field tilt – A new concept for location of potential field sources. Journal of Applied Geophysics. 1994;32:213–217.
30. Narayan S, Sahoo SD, Pal SK, Kumar U, Pathak VK, Majumdar TJ, Chouhan A. Delineation of structural features over a part of the Bay of Bengal using total and balanced horizontal derivative techniques. Geocarto Int. 2016;32(1):1–16.
31. Pal SK, Narayan S, Majumdar TJ, Kumar U. Structural mapping over the 85E ridge and surroundings using EIGEN6C4 high resolution global combined gravity field model: An integrated approach. Mar. Geophys. Res. 2016b;37:159–184.
DOI: 10.1007/s11001-016-9274-3
32. Pal SK, Majumdar TJ. Geological appraisal over the Singhbhum-Orissa Craton, India using GOCE, EIGEN6-C2 and in-situ gravity data; Int. J. Appl. Earth Obs. Geoinf. 2015;35:96–119.
33. Oruc B, Selim HH. Interpretation of magnetic data in the Sinop area of Mid Black Sea, Turkey, using tilt derivative, Euler deconvolution, and discrete wavelet transform. Journal of Applied Geophysics. 2011;74:194–204.
34. Reid AB, Allsop JM, Granser H, Millet AJ, Somerton IW. Magnetic interpretation in three dimensions using Euler decon-volution. Geophysics. 1990;55:80-91.
35. Thompson DT. EULDPH: A new technique for making computer-assisted depth estimates from magnetic data. Geophysics. 1982;47:31–37.
36. Tarlowski C, Gunn PJ, Mackey T. Enhancements of the magnetic map of Australia. AGSO Journal of Australian Geology and Geophysics. 1997;17(2):77-82.
37. Reeves C. Aeromagnetic surveys, principle practice and interpretation. Geosoft E-Publication; 2005.
Available:www.geosoft.com/media/uploads/resources/technical/aeromagnetic_survey_Reeeves.pdf
38. Keating PB. A simple technique to identify magnetic anomalies due to Kimberlite pipes. Exploration and Mining Geology. 1995;4(2):121–125.
39. Gunn PJ, Dentith MC. Magnetic responses associated with mineral deposits. AGSO Journal of Australian Geology and Geophysics. 1997;17:145-158.
40. Hood P, McClure DJ. Gradient measure-ments in ground magnetic prospecting. Geophysics. 1965;30(3):403-410.
41. Sharma PV. Environmental and engineering geophysics. Cambridge University Press, United Kingdom; 2002.

42. Isles DD, Rankin LR. Geological interpretation and structural analysis of aeromagnetic data. TGT Consulting/ Geointerp Unpublished workshop manual; 2011.
43. Ajakaiye DE, Hall DH, Miller TW, Verherjen PJT, Awad MB, Ojo SB. Aeromagnetic anomalies and tectonic trends in and around the Benue Trough Nigeria. Nature. 1986;319:582-584.
44. Ananaba SE. Dam sites and crustal megalineaments in Nigeria. ITCJ. 1991;1: 26-29.
45. Haruna IV. Review of the Basement Geology and Mineral Belts of Nigeria. Journal of Applied Geology and Geophysics (IOSR-JAGG) e-ISSN: 2321–0990, p-ISSN: 2321–0982. 2017;5(1)Ver. I: 37-45

Peer-review history:
The peer review history for this paper can be accessed here:
http://www.sdiarticle4.com/review-history/58030